IEEE Photonics Journal
An IEEE Photonics Society Publication

Open Access

Broadband Spurious-Free Dynamic Range Expander for Microwave Photonic Links Based on Optical Distortion Control

Volume 11, Number 1, February 2019

Tianwei Jiang
Jianming Shang
Song Yu
Xinmeng Ye
Wanyi Gu

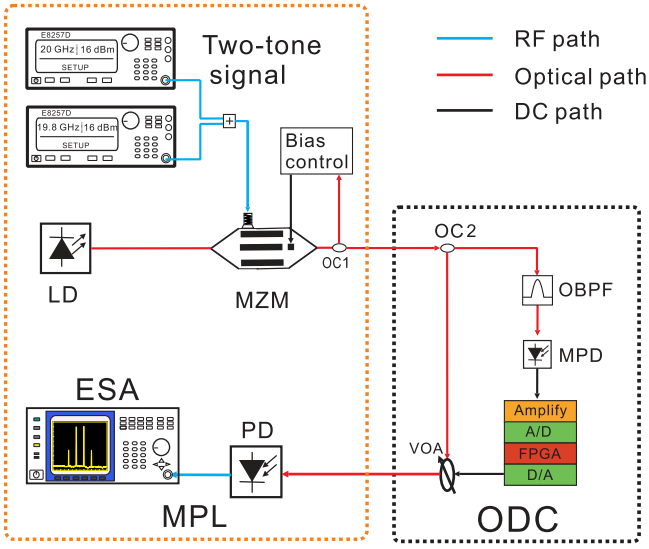

DOI: 10.1109/JPHOT.2019.2894568
1943-0655 © 2019 IEEE

Broadband Spurious-Free Dynamic Range Expander for Microwave Photonic Links Based on Optical Distortion Control

Tianwei Jiang, Jianming Shang, Song Yu, Xinmeng Ye, and Wanyi Gu

State Key Laboratory of Information Photonics and Optical Communications, Beijing University of Posts and Telecommunications, Beijing 100876, China

DOI:10.1109/JPHOT.2019.2894568

Manuscript received September 21, 2018; revised December 12, 2018; accepted January 16, 2019. Date of publication January 31, 2019; date of current version February 11, 2019. This work was supported in part by the National Natural Science Foundation of China under Grant 61531003, Grant 61690195, Grant 61701040, and Grant 61427813; in part by the Fund of State Key Laboratory of Information Photonics and Optical Communications [Beijing University of Posts and Telecommunications (BUPT)]; in part by the Youth Research and Innovation Program of BUPT under Grant 2017RC13; and in part by the Open Funds of IPOC under Grant IPOC2017ZT14. Corresponding author: Song Yu (e-mail: yusong@bupt.edu.cn).

Abstract: A wideband spurious-free dynamic range (SFDR) expander that uses optical distortion control technique is proposed in this study for microwave photonic links. A third-order intermodulation distortion (IMD3), which is sensed by extracting the modulated optical carrier, will be monitored and attenuated adaptively by controlling the optical power injected into the photodetector. Therefore, the IMD3 can be suppressed below the noise floor (NF), and the SFDR can be expanded further. In addition, the sensing signal stems from the modulated optical carrier, which is independent of radio frequency. Thus, our system is essentially a broadband system whereby the dynamic range expander is applied to classical intensity modulation and direct detection microwave photonic link. Experimental results demonstrate that the SFDR is improved from 46.84 to 67.98 dB/Hz$^{2/3}$ with a −70 dBm noise power. The SFDR can even reach 150 dB/Hz$^{2/3}$ with a bandwidth of 36 GHz with a 1 Hz NF.

Index Terms: Microwave photonics, microwave photonics signal processing, dynamic range.

1. Introduction

Microwave photonic links (MPLs) that offer low loss, large bandwidth and electromagnetic interference immunity are required for various applications, such as radars, wireless communications, phased array antennas, and warfare systems [1]. A key figure of merit for MPLs is their spurious free dynamic range (SFDR) defined as the range of input powers over which the output signal is above the output noise floor (NF), and all the spurious signals are less than or equal to the output NF [2]. The minimum input power is limited by carrier-to-noise ratio (CNR), which is typically determined by the electrical and optical devices [3]–[5]; whereas the maximum input power must be improved by optimizing the system structure to suppress the spurious signals.

In recent years, considerable efforts have been placed on two perspectives in designing structures with a high SFDR. One perspective focuses on linearization to the MPLs itself by constructing a compensation path in an optical domain using different optical dimensions, such as intensity [6], [7],

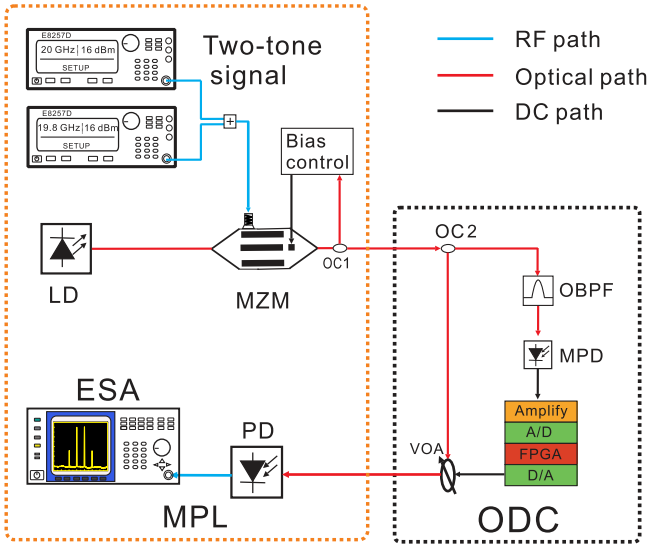

Fig. 1. ODC-based SFDR expander method applied to an IMDD link. The orange dotted square diagram represents the traditional IMDD-MPL, and the black dotted square diagram is the proposed ODC dynamic range expander. The blue solid line represents the radio frequency path, The red solid line is the optical path, and the black line transports the DC voltage information.

phase [8], polarization [9], and wavelength [10]. By using these approaches, wideband MPLs with SFDRs of more than 120 $dB/Hz^{2/3}$ have been reported. However, the other approach is promising to obtain SFDRs beyond 130 $dB/Hz^{2/3}$. The other perspective focuses on constituting external dynamic range expanders, such as digital compensation [11]–[14], and phase-tracking loop [15]–[18]. However, digital compensation techniques are limited by quantization noise and processing bandwidth. The phase tracking loop method can increase the SFDR to 148 $dB/Hz^{2/3}$ [18], although it is also limited by the bandwidth narrowness caused by the loop delay. Thus, the broadband dynamic range expander is quite promising, but has not been reported.

In fact, the relationship between the power of the optical carrier and the modulation depth follows a monotone decreasing $J_0(x)$ Bessel function. The optical carrier can be extracted for the sensing modulation depth, which is related to the third-order intermodulation (IMD3). We propose and experimentally demonstrate an optical distortion control (ODC)-based broadband SFDR expander for MPLs. In practice, we use an optical filter to extract the optical carrier, which is converted to a variable direct current (DC) signal. The DC signal is processed electrically and drives a variable optical attenuator (VOA), which is placed before the optical to electrical (O/E) demodulation. Thus, IMD3 will constantly be suppressed below the NF. Hence, thereby increasing the SFDR. Our ODC based SFDR expander is a wideband system because the sensing signal is extracted from the optical carrier, that is independent of the radio frequency (RF). In the experiment, we use the traditional intensity modulation and direct detection (IMDD) link as an example. The results demonstrate that the SFDR can increase from 46.84 $dB/Hz^{2/3}$ to 67.98 $dB/Hz^{2/3}$ with a -70 dBm noise power through our method. A record SFDR of more than 150 $dB/Hz^{2/3}$ across 36 GHz (from 4 GHz to 40 GHz) with a 1 Hz NF has been achieved.

2. Topology and Principle of Operation

Fig. 1 illustrates a conceptual diagram of our ODC-based SFDR expander applied to a conventional IMDD link. The IMDD system is composed of a laser diode (LD), a Mach-Zehnder modulator (MZM), an optical circulator (OC1), a bias control circuit, and a photodetector (PD). OC1 and the control circuit comprise a bias control loop, which is used to avoid the DC drift phenomena. Our ODC

modular is placed after the bias control loop. In the ODC modular, a modulated lightwave is divided into two parts by a single mode optical coupler (OC2). The signal path with the most optical power is used for recovering the RF signal. The monitor path with the fewest optical powers is used for monitoring the modulation depth and providing the control signal. In the monitor path, the lightwave is injected into an optical bandpass filter (OBPF). The center wavelength of the OBPF is set to be the same as the optical carrier. Thus, the optical carrier is extracted. A monitor PD (MPD) converts an optical carrier into an electrical DC information. This information represents the modulation depth of the MZM that follows the Bessel function. An electrical circuit is used to map the relation between the DC information and the controlling signal. This circuit contains an analog-to-digital converter, field programmable gate array (FPGA), and a digital-to-analog converter. With specific amplification, the output signal drives an microelectromechanical system (MEMS)-based VOA in the signal path. Thus, the optical power injected into the PD can be automatically attenuated followed by the input of the RF power. Our ODC will activate when the RF power is sufficiently large to generate a large IMD3 that is above the NF. Optical power is attenuated by a specific radio. The IMD3 is attenuated below than the NF. Therefore, the system can receive a large RF power without The IMD3, and the SFDR is improved. Generally, the process can be described in six steps.

1) A continuous wave lightwave is modulated in a traditional intensity modulation. Then, two sidebands will be generated in the optical domain.
2) The modulated optical signal is split into two paths, and an additional monitor path is obtained.
3) In the monitor path, an optical filter is used to extract the optical power of the optical carrier, which is related to the modulation depth in the previous modulation process.
4) This optical power information is converted into an electrical signal by a photodiode. Then, the electrical signal is converted by an analog to digital convertor and processed by an FPGA.
5) The output voltage of the FPGA feed is forwarded to a VOA.
6) A PD recovers the RF signal. Given the VOA, the IMD components will be decreased below the NF. Thus, the SFDR will be increased remarkably.

Mathematically, a two-tone RF with an angular frequency of ω_1 and ω_2 modulates the MZM. An optical field at the output of the MZM can be expressed as follows:

$$u(t) = \sqrt{P_o} e^{j\omega_O t} sin\{\theta + \beta[sin(\omega_1 t) + sin(\omega_2 t)]\}, \tag{1}$$

where P_0 represents the optical power of the LD, ω_O represents the angular frequency of the optical carrier; $\beta = \pi \frac{V_{RF}}{V_\pi}$ is the modulation depth of each RF signal, V_{RF} is the amplitude of each RF signal, V_π is the half wave voltage of the MZM, $\theta = \pi \frac{V_{DC}}{V_\pi}$ is the optical phase difference between the arms, and V_{DC} is the DC voltage used on the MZM. Based on the Jacobi-Anger expansion, the envelope of the signal in Eq. 1 can be expanded as follows:

$$\begin{aligned} u(t) = \sqrt{P_o} e^{j\omega_O t} \{ & sin(\theta)[J_0^2(\beta) \pm 2J_1^2(\beta) cos(\omega_1 \pm \omega_2)t \\ & + 2J_0(\beta)J_2(\beta) cos(2\omega_{1,2}t) + \ldots)] \\ & + cos(\theta)[2J_0(\beta)J_1(\beta) sin(\omega_{1,2})t \\ & \pm 2J_1(\beta)J_2(\beta) sin(2\omega_{1,2})t + \ldots]\}, \end{aligned} \tag{2}$$

where J_l is the Bessel function of the first kind of order l. Through the passing VOA with the attenuated power of $\alpha(V_c)$, the microwave signal is recovered by the PD. α is a monotonic function that represents the attenuate function of VOA. V_c is the control voltage added to the VOA. The output current is given as follows:

$$\begin{aligned} I(t) &= 4RP_o \frac{\alpha(V_c)}{\gamma} sin(\theta)[A(\beta) sin(\omega_{1,2}t) + B(\beta) sin(2\omega_{1,2} - \omega_{2,1})t] \\ A(\beta) &= J_0^3(\beta)J_1(\beta) + J_1^3(\beta)J_0(\beta) + J_0^2(\beta)J_1(\beta)J_2(\beta) \\ B(\beta) &= 2J_0^2(\beta)J_1(\beta)J_2(\beta) + J_1^3(\beta)J_0(\beta). \end{aligned} \tag{3}$$

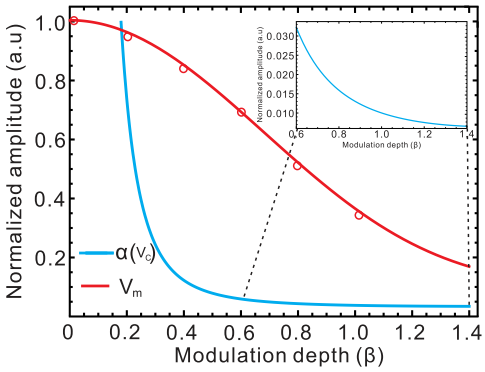

Fig. 2. Numerical simulation of the normalized V_m and $\alpha(V_c)$, when the modulator is biased at the quadrature point. The magnified $\alpha(V_c)$ at the range of 0.6 to 1.4 is shown in the upper right corner.

where γ is the power consumption caused by the OC2. To ensure that the power of the IMD3 is lower than or equal to the NF, the following equation is used:

$$\alpha(V_c) = \frac{\gamma}{4RP_o sin(\theta)B(\beta)}\sqrt{\frac{NF}{Z}}. \tag{4}$$

where NF represents the power of the NF,and Z is the impedance of the PD. On the basis of Eq.4, we can construct a relationship between the control voltage of the VOA and the modulation depth. In the monitor path, the optical carrier is filtered by an OBPF. After the MPD and amplifier circuit, the output DC component can be denoted as follows:

$$\begin{aligned} V_m &= 4ARP_o sin^2\left(\frac{\theta}{2}\right)C(\beta)Z, \\ C(\beta) &= J_0^4(\beta) + 2J_1^4(\beta). \end{aligned} \tag{5}$$

Let $\alpha(V_c) = f(V_m)$, $f(x)$ that is the transfer function of the FPGA, can be calculated using Eqs.4 and 5. To avoid control ambiguity, $f(x)$ must be verified monotonous. Let $A(\beta) = B(\beta)$, we can calculate that third order output intercept point occurred while $\beta = 1.31$. The numerical simulation results of V_m and $\alpha(V_c)$ are depicted in Fig. 2. Both functions are monotonic functions when $\beta \leq 1.31$. Thus, $f(x)$ will also be a monotonic function. In addition, if the RF input power increases by 1 dB, then the IMD3s will increase by 3 dB. Therefore, the SFDR can be improved by 50% through our ODC method.

To investigate the performance of the system with a realistic signal, we assume that a vector data signal is carried by the RF signal. The output signal can be expressed as follows:

$$I(t) = 4RP_o\frac{\alpha(V_c)}{\gamma}sin(\theta)[A(\beta * v_s)sin(\omega_{1,2}t + \varphi_s)], \tag{6}$$

where v_s represents the data signal added to the amplitude of the RF signal, φ_s is the data signal added to the phase of RF signal. In Eq. 6, the optical attenuation has no effect the phase-coded output signal. For the amplitude-coded signal, the optical attenuation will reduce signal-to-noise ratio (SNR) with the same β. However, the ODC is only activated when the β is sufficiently large. In this case, the SNR is increasingly large that the reduction in SNR is tolerant. The reduced SNR is the same as an unreduced signal with a low β. Thus, the reduce SNR is verified to be usable.

3. Experimental Results

We utilized the ODC-based IMDD link (Fig. 1) to verify our analysis and demonstrate the SFDR and bandwidth performance of the link. The optical source in our experiment was a distributed feedback laser (emcore 1782B) with high power and low relative intensity noise [19] which was driven by a

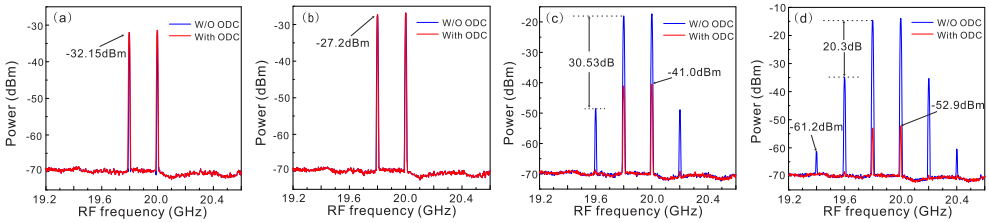

Fig. 3. Electrical spectrum of the output fundamental signal and IMD3s, with input RF powers of (a) −5 dBm, (b) 0 dBm, (c) 10 dBm, and (d) 15 dBm.

combination of a laser diode and a temperature controller (Newport, 6100). The driving current was set to 385.01 mA that allows the output optical power to be 19.35 dBm, and the wavelength is set to 1550.12 nm. A two-tone RF input signal set to 19.8 GHz and 20 GHz with a power of 10 dBm was injected into a lithium niobate single-drive MZM (Optilab, $V_\pi \sim 4V$@40 GHz). Then, a bias control circuit (PlugTech, MBC-Q-02) was used to maintain the MZM operation at the half-intensity point (quadrature). Then, a single-mode optical coupler (with a split ratio of 70:30) divided the modulated lightwave into two parts, wherein 70% was injected into a MEMS based VOA (OptiMems). The optical power injected into the PD without any attenuation was measured at 9 dBm. The VOA was an electrical drive device with high control accuracy and stable performance [20]. The driving voltage was generated from the monitor path, wherein the optical carrier was exacted by a fiber Bragg grating (FBG)-based optical filter (Teraxion) with a center wavelength of 1550.12 nm and a bandwidth of 2 GHz. A DC-coupled monitor PD converted the power of the optical carrier to monitor the analogy information, which was subsequently amplified and converted into digital signals by an ADC with an 8-bit resolution (AD9280). The digital signals is processed by a specific transfer function through an FPGA (Cyclone). We measured V_c and V_m to achieve the transfer function in the FPGA. The processed voltage (V_c) was converted back to analog voltage by a digital to analog convertor (DAC9708) to generate a suitable driving voltage applied to the VOA. Then, the ultimate RF output signal of the system was recovered through a high optical power handling photodetector with more than 40 GHz bandwidth (Discovery semiconductors, DSC20H-39). Electrical spectrum analyzers (ESA, *R*&*S*, and FSV40) were used for measuring.

We recorded the IMD3 power and the monitor voltage at the output of the electrical amplifier as the input RF power varied from −20 to 18 dBm. The calculated β and measured voltages are demonstrated in Fig. 2. The experimental results agreed with our theoretical analysis.

To illustrate the performance of the SFDR, we measured the RF power of the fundamental and IMD3 the as input RF powers that are varied discretely (Fig. 3). The red line represents the frequency component of the proposed ODC dynamic range expander; The blue line represents the frequency component without our ODC. The NF was set to −70 dBm by adjusting the resolution bandwidth of the ESA to 5 MHz and the attenuation to 35 dB. In Fig. 3(a) and (b), when the RF power was small, the IMD3 was below the NF. The red and blue lines nearly coincided, thereby indicating that our ODC is not activated. The entire system can be treated as a traditional IMDD link in this case. The IMD3 power increased versus the RF input power. The ODC strategy activated when the IMD3 power exceeded −70 dBm. The optical power injected into the PD was attenuated until IMD3 was reduced below −70 dBm again. The fundamental components decreased from −17.97 dBm to −41.0 dBm, as exhibited in Fig. 3(c) shows. With a high RF power, IMD3 and fifth-order modulation distortion (IMD5) would appear simultaneously (Fig. 3(d)). IMD3 and IMD5 were suppressed below the NF, after the ODC processing. Moreover, the processing speed was very fast. In spite of the large loss in the fundamental components, the CNR reached 17.1 dB.

Fig. 4(a) and (b) present the output power versus the input power for the noise powers −70 and −166 dBm (NF measured at 1 Hz), respectively. When our ODC operates, the IMD3s were constantly below the noise power and the fundamental components would decrease with a slope of −2. The two plots, showed that our ODC method can significantly improve the SFDR of the link.

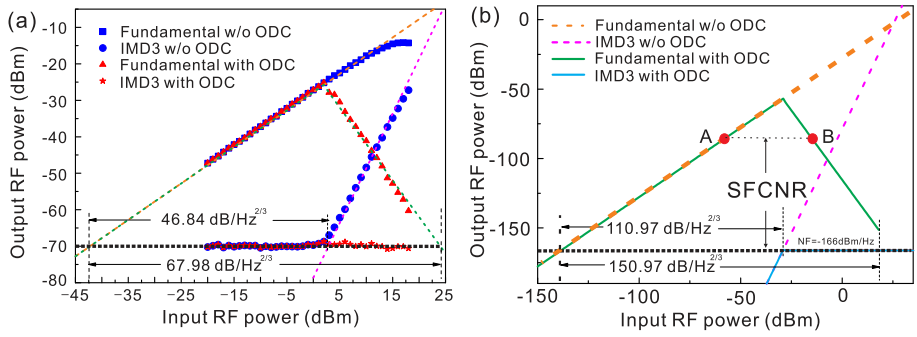

Fig. 4. Radio frequency (RF) output power of the fundamentals and third order intermodulation distortion components as a function of RF input power for the proposed ODC link. Two tone signals with frequency of 19.8 GHz and 20 GHz are used. (a) Spurious free dynamic range (SFDR) with −70 dBm noise power, (b) SFDR with noise floor of 1 Hz bandwidth.

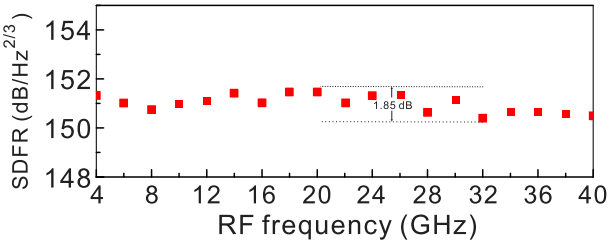

Fig. 5. Spurious free dynamic range response of proposed optical distortion control system with measured 1 Hz noise floor of -166 dBm.

For a −70 dBm noise power, the SFDR could be improved from 46.84 dB/Hz$^{2/3}$ to 67.98 dB/Hz$^{2/3}$. This improvement value agrees with the value predicted by the discussion above. For a measured 1 Hz NF, the ODC would activate earlier. Accordingly, our system had been limited by the sensitivity of the PD, which was −31 dBm in our experiment. Thus, the SFDR could reach 150.97 dB/Hz$^{2/3}$. The gain would dynamically decrease when our OAGC works. However, the system would continue to work properly despite this kind of dynamic decrease. Most of the mentioned in the introduction did not realize that, in actual scenario, the data were baseband signal multiplied on the RF carrier, rather than that in the RF carrier itself. No information was available on the dimension of the RF power. Thus, the gain did not have to be a constant value for the whole dynamic range. The operation performance was determined by the spurious-free CNR (SFCNR), rather than the gain. To enhance the SFCNR, we should suppress the noise for a small signal input and suppress distortion components for a large signal input. For the latter, the received signal was sufficiently large that we could sacrifice part of this large signal input to obtain the distortion suppression. The SFCNR was still sufficient, despite of the reduce in gain. For example, the Fig. 4(b) displays that our OAGC is eddective in point B, wherein the gain decreases, but the SFCNR remains the same as that in point A. This phenomenon was the case in a small signal input. Thus, the performance of point A and B were the same.

The bandwidth of the system was limited by the bandwidth of the modulator. A 40 GHz modulator (Optilab, IML-1550-40-G)was used to measure the operation bandwidth of the system. Fig. 5 presents the SFDR performance in different frequencies with 1 Hz NF. An SFDR beyond 150 $dB/Hz^{2/3}$ was achieved with a frequency from 4 GHz to 40 GHz. The fluctuation value was measured as 1.85 dB. Therefore, our ODC link is a broadband system. A 20 MB/s 16QAM signal loaded on a 12 GHz RF carrier was added to the system by a vector signal generator (Agilent, E8267D), to prove the ODC performance when a realistic signal is added to the radio frequency.

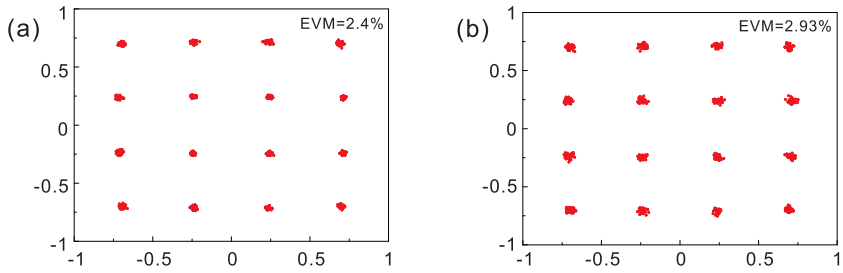

Fig. 6. (a) Constellation of the output signal when the input power is 4 dBm, and (b) 8 dBm.

Fig. 6 illustrates the constellations of the output signal with different modulation depth when the ODC is activated. The error vector magnitude was measured to be less than 3% thereby indicating a high potential for many applications.

4. Conclusion

We propose and experimentally demonstrate a wideband dynamic range expander on the basis of the distortion monitor in the optical domain. This method is an effective means of improving the SFDR performance for MPLs. In the proposed expander, the power of the IMD3 is monitored by the modulated optical carrier caused by their monotone relation. Then, the optical power injected into the PD is attenuated through a VOA that is driven by a processed monitor signal when the IMD3 power exceeds the noise power. Ultimately, the IMD3 power can be reduced again below the noise power. Theoretically, the SFDR can be improved by 50%. The experimental results demonstrate that a SFDR of 150.97 dB/Hz$^{2/3}$ can be achieved. A flat operation bandwidth is obtained from 4 GHz to 36 GHz.

References

[1] J. Capmany and D. Novak, "Microwave photonics combines two worlds," *Nat. Photon.*, vol. 1, no. 6, pp. 319–330, 2007.
[2] V. J. Urick, J. D. McKinney, and K. J. Williams, *Fundamentals of Microwave Photonics* (Wiley Series in Microwave and Optical Engineering). Hoboken, NJ, USA: Wiley, 2015, Ch. 2, pp. 45–46.
[3] Y.-G. Zhao, X. Luo, D. Tran, Q. Hang, P. Weber, and T. Hang, "High-power and low-noise DFB semiconductor lasers for RF photonic links," in *Proc. Avionics, Fiber Opt. Photon. Technol. Conf.*, Cocoa Beach, FL, USA, 2012, pp. 66–67.
[4] A. Beling, X. Xie, and J. C. Campbell, "High-power, high-linearity photodiodes," *Optica*, vol. 3, no. 3, pp. 328–338, 2016.
[5] L. S. Watkins *et al.*, "Low noise high power ultra-stable SS laser for 1550 nm," in *Proc. Avionics Fiber Opt. Photon. Technol. Conf.*, Annapolis, MD, USA, 2006, pp. 56–57.
[6] A. Karim and J. Devenport, "High dynamic range microwave photonic links for RF signal transport and RF-IF conversion," *J. Lightw. Technol.*, vol. 26, no. 15, pp. 2718–2724, 2008.
[7] J. Li, Y.-C. Zhang, S. Yu, T. Jiang, Q. Xie, and W. Gu, "Third-order intermodulation distortion elimination of microwave photonics link based on integrated dual-drive dual-parallel Mach-Zehnder modulator," *Opt. Lett.*, vol. 38, no. 21, pp. 4285–4287, 2013.
[8] Y. Cui *et al.*, "Intermodulation distortion suppression for intensity-modulated analog fiber-optic link incorporating optical carrier band processing," *Opt. Exp.*, vol. 21, no. 20, pp. 23433–23440, 2013.
[9] M. Huang, J. Fu, and S. Pan, "Linearized analog photonic links based on a dual-parallel polarization modulator," *Opt. Lett.*, vol. 37, no. 11, pp. 1823–1825, 2012.
[10] B. M. Haas, V. J. Urick, J. D. McKinney, and T. E. Murphy, "Dual-wavelength linearization of optically phase-modulated analog microwave signals," *J. Lightw. Technol.*, vol. 26, no. 15, pp. 2748–2753, 2008.
[11] D. Lam, A. M. Fard, B. Buckley, and B. Jalali, "Digital broadband linearization of optical links," *Opt. Lett.*, vol. 38, no. 4, pp. 446–448, 2013.
[12] R. Zhu, X. Zhang, B. Hraimel, D. Shen, and T. Liu, "Broadband predistortion circuit using zero bias diodes for radio over fiber systems," *IEEE Photon. Technol. Lett.*, vol. 25, no. 21, pp. 2101–2104, Nov. 2013.
[13] Y. Pei *et al.*, "Complexity-reduced digital predistortion for subcarrier multiplexed radio over fiber systems transmitting sparse multi-band RF signals," *Opt. Exp.*, vol. 21, no. 3, pp. 3708–3714, 2013.
[14] T. R. Clark and M. L. Dennis, "Coherent optical phase-modulation link," *IEEE Photon. Technol. Lett.*, vol. 19, no. 16, pp. 1206–1208, Aug. 2007.
[15] H.-F. Chou *et al.*, "Highly linear coherent receiver with feedback," *IEEE Photon. Technol. Lett.*, vol. 19, no. 12, pp. 940–942, Jun. 2007.

[16] D. Zibar, L. A. Johansson, H.-F. Chou, A. Ramaswamy, and J. E. Bowers, "Dynamic range enhancement of a novel phase-locked coherent optical phase demodulator," *Opt. Exp.*, vol. 15, no. 1, pp. 33–44, 2007.
[17] S. Jin, L. Xu, P. Herczfeld, A. Bhardwaj, and Y. Li, "Recent progress in attenuation counterpropagating optical phase-locked loops for high-dynamic-range radio frequency photonic links," *Photon. Res.*, vol. 2, no. 4, pp. B45–B53, 2014.
[18] A. Ramaswamy, "A linear coherent integrated receiver based on a broadband optical phase-locked loop," Ph.D. thesis, Univ. California, Santa Barbara, 2010, pp. 46–47.
[19] J.-S. Huang, H. Lu, and H. Su, "Ultra-high power, low RIN and narrow linewidth lasers for 1550nm DWDM 100km long-haul fiber optic link," in *Proc. 21st Annu. Meeting IEEE Lasers Electro Opt. Soc.*, Newport Beach, CA, USA, 2008, pp. 894–895.
[20] X. M. Zhang, A. Q. Liu, C. Lu, and D. Y. Tang, "MEMS variable optical attenuator using low driving voltage for DWDM systems," *Electron. Lett.*, vol. 38, no. 8, pp. 382–383, 2002.